HNPS Advances in Nuclear Physics

Vol 25 (2017)

HNPS2017

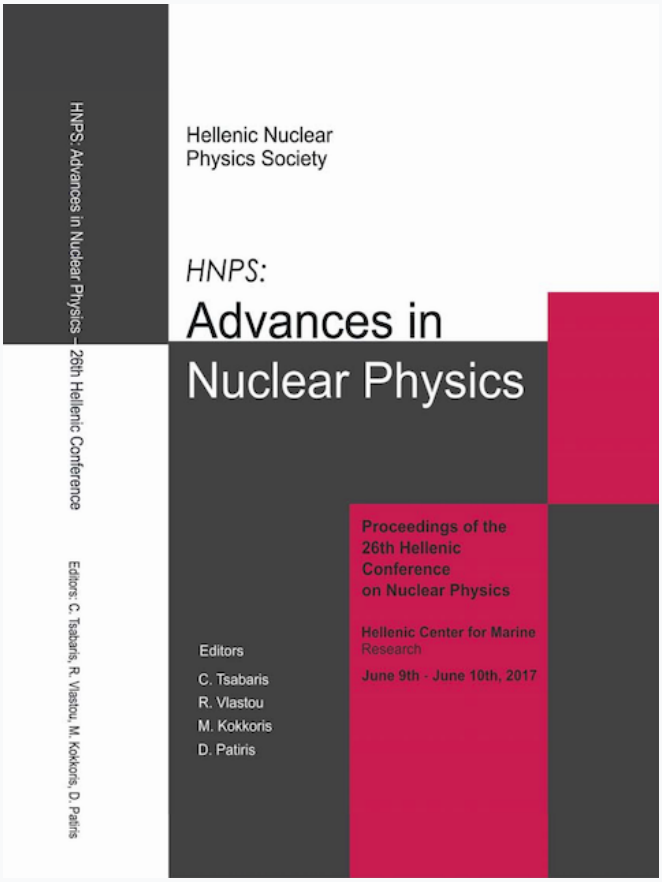

Measurements of the 234U(n,f) cross section using quasimonoenergetic beams in the keV and MeV range and a Micromegas detector assembly

A. Stamatopoulos, A. Kanellakopoulos, A. Kalamara, A. Tsinganis, M. Diakaki, M. Kokkoris, V. Michalopoulou, M. Axiotis, A. Lagoyannis, R. Vlastou

doi: 10.12681/hnps.1971

Measurements of the ^{234}U(n,f) cross-section using quasi-monoenergetic beams in the keV and MeV range and a Micromegas detector assembly

A. Stamatopoulos[1,*] , A. Kanellakopoulos[1], A. Kalamara[1], A. Tsinganis[2], M. Diakaki[1,2], M. Kokkoris[1], V. Michalopoulou[1], M. Axiotis[3], A. Lagoyiannis[3], R. Vlastou[1]

[1] National Technical University of Athens, Department of Physics, Zografou Campus, Athens, 15780, Greece

[2] European Organisation for Nuclear Research (CERN), CH-1211 Geneva 23, Switzerland

[3] *Tandem Accelerator Laboratory, Institute of Nuclear and Particle Physics, N.C.S.R. Demokritos, Patr. Gregoriou E & 27 Neapoleos Str, 15341 Agia Paraskevi, Greece*

Abstract The ^{234}U(n,f) cross-section has been measured at incident neutron energies of 452 keV and 8.7 and 10 MeV using the ^{7}Li(p, n) and the ^{2}H(d, n) neutron production reactions respectively, relative to the ^{235}U(n, f) and ^{238}U(n, f) reference reactions. The measurement was carried out at the neutron beam facility of N.C.S.R. "Demokritos", using a set-up based on the Micromegas detector. The actinide samples were characterised, in terms of mass and contaminations, via α-spectroscopy using a surface barrier silicon detector set-up. The neutron flux at the actinide targets has been thoroughly studied by coupling the NeuSDesc and MCNP5 codes, taking into account the energy and angular straggling of the primary ions in the neutron production sources in addition to contributions from competing reactions and neutron scattering in the surrounding materials. Auxiliary Monte-Carlo simulations were performed with the FLUKA and GEF codes, to determine the fission fragment detection efficiency. Emphasis is given on the full covariance propagation and the estimation of the total uncertainty. The final results are also presented.

Keywords ^{234}U, fission, cross-section, Micromegas detector, MCNP5, covariance

INTRODUCTION

The accurate knowledge of neutron-induced fission cross-sections of minor actinides and other isotopes involved in the nuclear fuel cycle, are essential for the optimum design of advanced nuclear systems based either on fast or slow neutron spectra as well as for the reduction of safety margins of existing and future conventional facilities. Such experimental data can also provide the necessary feedback for the adjustment of nuclear model parameters used in the evaluation process, resulting in further developments of nuclear fission models.

The study of ^{234}U(n,f) is considered to be important since ^{234}U is involved in the thorium cycle, which is one of the possible fuel cycles to be used in advanced generation-IV reactors and accelerator-driven systems [1], where it builds up from neutron capture in ^{233}U, acting as ^{240}Pu in the conventional uranium cycle.

In this context, several cross-section measurements have been presented over the past years, mainly using the time-of-flight technique, covering a large energy range from thermal

to fast neutron energies [2-13]. As seen in fig. 1, discrepancies between experimental data and latest evaluations are present that reach up to 30% in the fission subthreshold region and 15% in the second-chance fission plateau.

In an attempt to clarify the discrepancies seen in the aforementioned neutron energy regions, new measurements of the ^{234}U(n,f) cross section, were performed with quasi-monoenergetic neutron beams, using the samples from Karadimos et al. [13] campaign.

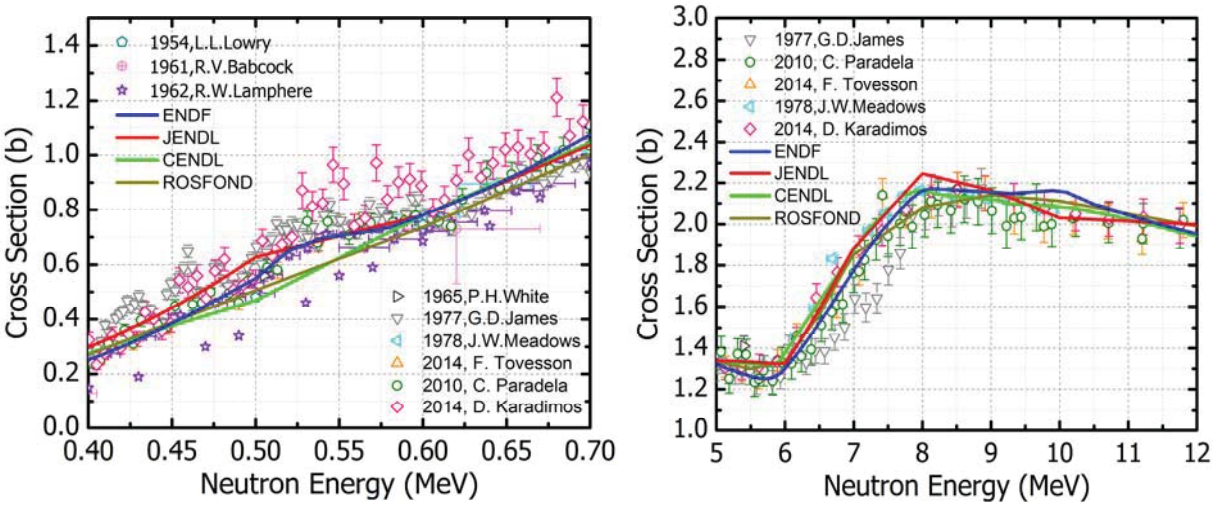

Fig. 1. Available ^{234}U(n,f) literature data and latest evaluations in the fission subthreshold region (left) and in the second-chance fission plateau (right).

EXPERIMENTAL DETAILS

Neutron production

The experiment was carried out at the neutron facility of the Institute of Nuclear and Particle Physics of the NCSR "Demokritos" using the 5.5 MV Tandem Van de Graaf accelerator [14, 15]. Depending on the energy region of interest, the most suitable neutron production reaction was used. More specifically, for the data point at 452 keV the ^{7}Li(p,n)^{7}Be reaction was used since it yields a clean neutron spectrum for neutron energies up to 500 keV. The neutron source assembly consisted of a thin circular lithium fluoride (LiF) deposit (55 μgr/cm^2) of 2.2 cm diameter that was evaporated on a 500 μm-thick Tantalum backing, that also served as a beam stop for the incident protons. During the irradiations the LiF foil was kept at high vacuum (4 x 10^6 atm) and was placed on a stainless steel flange. To prevent any possible heat dissipation to the LiF foil caused by the high density energy transfer by the proton beam, a constant air-jet was applied to the flange that was housing the target assembly.

In the MeV region the ^{2}H(d,n)^{3}He reaction, commonly reffered to as the D-D reaction, was used to produce the neutron beam. The production target in this case, was a 3.7 cm long cylindrical cell with a diameter of 1 cm, filled with deuterium gas at a controlled preasure of 1.2 bar. The gas cell was fitted with a 5 μm-thick molybdenum window, which was also cooled by a cold air-jet, and a 1 mm-thick platinum beam stop. The produced neutron

spectrum in this case is less mono-energetic due to the parasitic reactions that occur from the deuteron beam (deuteron break-up and deuteron-induced reactions in the surrounding materials). To experimentally quantify these parasitic neutrons, data was taken with and without the deuterium gas. In both cases additional moderation tails are present occurring from the scattering of the primary neutrons with the surrounding materials, whose contribution was taken into account in the analysis using Monte-Carlo simulations.

Detectors

The measurements were carried out using a set-up based on the compact and low-mass microbulk variant [16-18] of the Micromegas (Micro-Mesh Gaseous Structure) gaseous detector [19–21]. Its active volume is divided into two parts by a thin, conductive, 50 μm pitched micro-mesh : a drift region (8 mm) and a narrow amplification gap (50 μm), in which a high electric field causes an avalanche multiplication. A scheme of the Micromegas layout is seen in fig. 2. Typical operating fields are in the order of 1 kV/cm and 100 kV/cm respectively, depending on the dielectric strength of the gas mixture, which in this case was a mixture of Ar : CO_2 (85:15) at a slightly atmospheric overpressure and room temperature. The detector set-up consisted of three similar detectors in total (1 for the ^{234}U sample, 1 for the ^{235}U reference sample and 1 for the ^{238}U reference sample), all of which were housed in a cylindrical aluminum chamber.

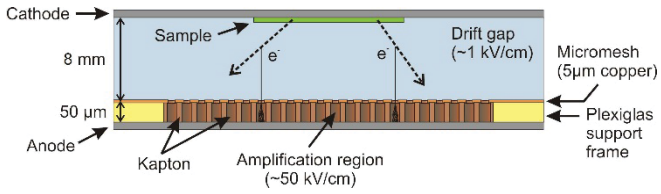

Fig. 2. A schematic layout of the microbulk Micromegas detector, whose volume is divided into two regions by a thin and conductive micro-mesh. The primary electrons drift towards the micromesh and are then multiplied inside the amplification region.

The signals produced by the detectors were recorded using a typical read-out chain consisting of ultra low gain pre-amplifiers, standard spectroscopy amplifiers and ADCs. This read-out layout provided a reasonable energy resolution needed for this kind of measurements, providing an adequate particle and fission fragment separation. A typical pulse height spectrum can be seen in fig. 3.

Fission foils

The fission foils used in the measurements (^{234}U as the measured sample, ^{235}U and ^{238}U as reference samples in the keV and MeV irradiations, respectively), were thin disks of 5.2 cm in diameter deposited on a 100 μm Al backing and produced at IPPE (Obninsk) and JINR (Dubna) via the painting technique. The total mass of each sample was accurately determined with α-spectroscopy using a set-up based on a Silicon Surface Barrier detector. The total

masses measured were 2.87(3), 5.00(8) and 9.82(26) mg for ^{234}U, ^{235}U and ^{238}U, respectively. In addition the samples were masked by 0.6mm thick aluminum disks with an inner diameter of 5 and 4 cm for the reference samples and the ^{234}U, respectively, in order to ensure a ±5° angular acceptance with respect to the neutron beam, thus minimising the uncertainty in the main energy of the incident neutron spectrum.

DATA ANALYSIS

The cross section calculation is based on the neutron flux determination on the samples as well as on the estimation of the true fission yield. Details on the analysis can be found in [22, 23] since emphasis will be given on the calculation of the covariance matrix.

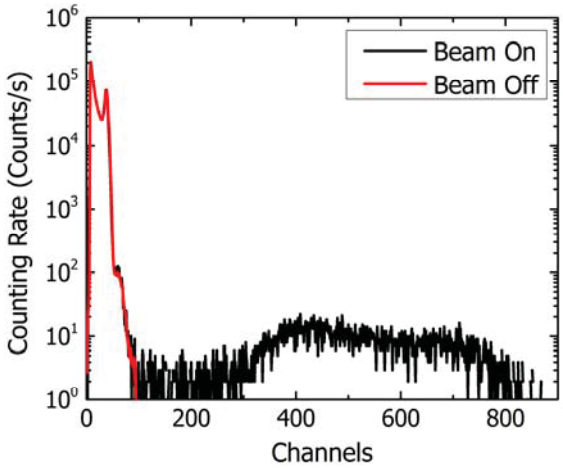

Fig. 3. Typical ^{235}U pulse height spectrum recorded during the 452 keV irradiation. A typical time-normalised beam-off spectrum is superimposed, to indicate the maximum energy deposited in the detector by the α-activity of the actinide sample.

Neutron flux

Prior to the determination of the neutron field on the ^{234}U sample, the neutron flux on the reference samples had to be calculated using eq. (1)

$$\Phi^{(ref)} = \frac{Y^{(ref)} f_{amp}^{(ref)} f_{DT}^{(ref)} f_{out/in}^{(ref)} f_{par}^{(ref)} f_{abs}^{(ref)}}{\mathrm{m}^{(\mathrm{ref})}\sigma^{(ref)}} \quad (1)$$

where

$Y^{(ref)}$ is the raw fission yield recorded by the detectors.

$f_{amp}^{(ref)}$ is the correction due to the amplitude cut introduced in the analysis to discriminate fission fragments from α-particles and was calculated using the GEF [24] and FLUKA [25] Monte Carlo codes.

$f_{DT}^{(ref)}$ is the acquisition dead-time correction.

$f_{out/in}^{(ref)}$ is the correction from the gas-out measurements that accounts for the ion-beam induced reactions that produce neutrons (only applicable where the DD reaction was used).

$f_{par}^{(ref)}$ is the correction factor to the fission yield due to the parasitic neutrons originating from the primary neutron spectrum.

$f_{abs}^{(ref)}$ is the correction factor due to the self-absorption of fission fragments in the sample itself and was calculated using the GEF and FLUKA Monte Carlo codes.

$m^{(ref)}$ is the number of atoms in the sample.

$\sigma^{(ref)}$ is the standard neutron cross section for ^{235}U and ^{238}U (n,f) obtained from [26].

The most important correction factor to be discussed is the f_{par} which was calculated as the ratio between the reaction rate below the parasitic energy E_{par} and the total reaction rate in the whole energy region as seen in eq. (2). The neutron flux used in the reaction rate calculation was determined by coupling the SRIM [27], NeuDesc [28] and MCNP5 [29] codes taking into account the energy and angular straggling of the primary ions in the neutron production sources in addition to contributions from competing reactions and neutron scattering in the surrounding materials. To ensure a detailed simulation a total of 10^9 primary neutrons were propagated and the neutron fluence was scored on the actinide samples for neutron energies that reach down to the thermal point with an isolethargic binning of 1000 bins per decade. In addition, the calculation of the standard cross sections on the isolethargic bins, was performed using a linear interpolation between evaluated points.

$$f_{par}^{(ref)} = \frac{\sum_{E_{par}} \sigma(E)\Phi(E)}{\sum_{E} \sigma(E)\Phi(E)} \quad (2)$$

The neutron flux Φ on the ^{234}U samples was propagated from the reference flux using the performed Monte Carlo simulations. More specifically, the ratio between the simulated fluxes on the ^{234}U sample and the reference one, provided a correction factor f_{MCNP} which was applied to the determined flux calculated from eq. (1) to estimate the neutron flux on the ^{234}U sample as seen in eq. (3).

$$\Phi = f_{MCNP}\Phi^{(ref)} \quad (3)$$

Cross section calculation and full covariance propagation

The neutron induced fission cross section σ of ^{234}U was calculated using eq. (4) in which the same notation as in eq. (1) is used. The values obtained along with the corresponding total estimated uncertainties can be seen on table 2 along with the correction factors and their uncertainties.

$$\sigma = \frac{Y\, f_{amp}\, f_{DT}\, f_{out/in}\, f_{par}\, f_{abs}}{m\, \Phi} \quad (4)$$

The total uncertainty in the cross section was calculated by means of full covariance propagation taking into account the parameters x_k[2] that contribute to the cross section calculation. For the uncorrelated parameters Y, f_{amp}, f_{DT}, $f_{out/in}$, f_{abs} and f_{MCNP}, for both the ^{235,8}U and ^{234}U sample, the uncertainties were tabulated in diagonal covariance matrices $\mathbf{V_k}$ where the matrix elements $(V_k)_{ii}$ had a value of the squared absolute uncertainty for each parameter. The size of each $\mathbf{V_k}$ matrix is directly related to the number of irradiations, which in this case were six, therefore each one had 6×6 dimensions. The number of $\mathbf{V_k}$ matrices is

[2] x_k describes the element of the vector **X** = [Y, f_{amp}, f_{DT}, $f_{out/in}$, f_{abs}, f_{par}, m, σ] for the neutron fluence on the reference samples and **X** = [Y, f_{amp}, f_{DT}, $f_{out/in}$, f_{abs}, f_{par}, m, f_{MCNP}, Φ] for the ^{234}U(n,f) cross section calculation.

related to the number of parameters used in the cross section calculation.

For the estimation of the covariance matrix $\mathbf{V_{fpar}}$ of the f_{par} parameter, the covariance matrix $\mathbf{V_{RR}}$ of the reaction rate $\Phi(E)*\sigma(E)$ had to be calculated which consisted of two sub-matrices : At the upper left corner the $\mathbf{V_{\Phi MCNP}}$ which was a diagonal matrix with the squared absolute uncertainties in the diagonal as given by MCNP and at the bottom right corner the $\mathbf{V_{lin}}$ which was the covariance matrix of the linear interpolated cross sections. The cross section $\sigma_i^{(lin)}$ at a given energy E_i, which lies between the E_j and E_{j+1} evaluated energies, was calculated using the evaluated cross sections $\sigma^{(eval)}$ as shown in eq. (5)

$$\sigma_i^{(lin)} = \frac{\sigma_j^{(eval)} - \sigma_{j+1}^{(eval)}}{E_j - E_{j+1}} \left(E_i - E_j\right) + \sigma_j^{(eval)} \qquad (5)$$

The $\mathbf{V_{lin}}$ matrix was calculated as the matrix product $\mathbf{G_{lin}} * \mathbf{V_{\sigma eval}} * \mathbf{G^T_{lin}}$ where $\mathbf{V_{\sigma eval}}$ was the evaluated covariance matrix obtained from [30] and $\mathbf{G_{lin}}$ was the sensitivity matrix (or Jacobian) with matrix element $(G_{lin})_{ij} = \partial\sigma_i^{(lin)}/\partial\sigma_j^{(eval)}$. The superscript "T" denotes the transpose matrix. The size of the sensitivity matrix $\mathbf{G_{lin}}$ depends on the defined number of points used in the simulation (number of rows) as well as on the given evaluated points (number of columns). In the present case, $\mathbf{G_{lin}}$ had 8000 rows and 160 columns therefore a specialized code was developed to handle such large dimensions as well as to visualize the final covariance and correlation matrices[3]. Figure 4 shows the resulting correlation matrices in the case of ^{235}U and ^{238}U (n,f). Finally the covariance matrix $\mathbf{V_{fpar}}$ was calculated as the product $\mathbf{G_{fpar}} * \mathbf{V_{RR}} * \mathbf{G^T_{fpar}}$ where $\mathbf{G_{fpar}}$ was the sensitivity matrix for the pararasitic factor f_{par} in each energy E_i (in this case i=6) and its elements were computed as follows: $(G_{fpar})_{ij} = \partial f_{par\,i}/\partial x_j$ where $x_j = \Phi_1, \Phi_2, \ldots, \Phi_N, \sigma_1, \sigma_2, \ldots, \sigma_N$ and N is equal to the number of isolethargic bins. The off-diagonal terms were 3 – 20 orders of magnitude smaller that the variance of the parasitic factors f_{par}, therefore they were proven to be practically uncorrelated. The total estimated uncertainties of the parasitic factors f_{par} can be seen in Table 1.

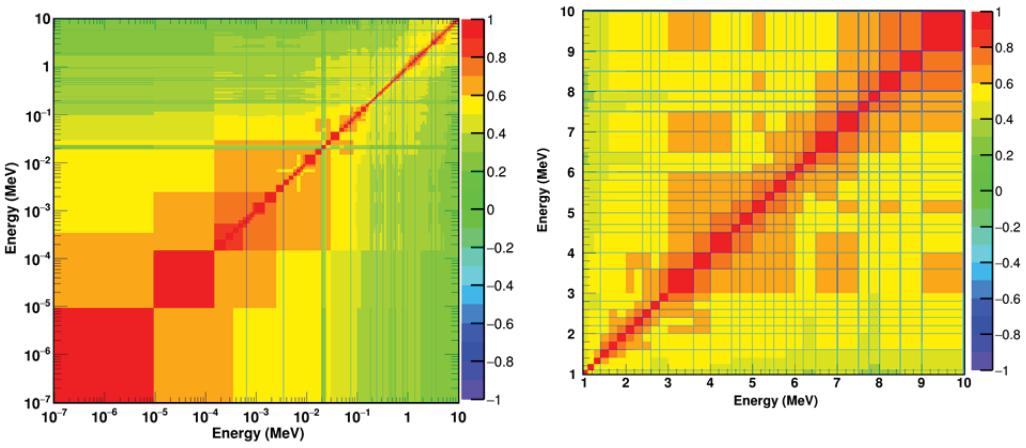

Fig. 4. Correlation matrix for the linear interpolated cross sections in an isolethargic binning of 1000 bins per decade in the case of ^{235}U(n,f) (left) and ^{238}U(n,f) (right). Both matrices were calculated by a specialized code that was developed in the framework of the present work.

[3] The ij-element of a correlation matrix **ρ** can be directly calculated from the covariance matrix **v** : $\rho_{ij} = v^2_{ij}/\sqrt{v_{ii}}\,\sqrt{v_{jj}}$

The covariance matrices of the masses $\mathbf{V_m}$ were directly calculated from the correlation matrices for all samples. Since the ^{234}U sample used in all six irradiations was the same, the correlation matrix elements had the value 1, therefore the diagonal elements were the squared absolute uncertainties while the off-diagonal had the value of the absolute uncertainty. For the reference samples, each of which was used only in three irradiations, the covariance matrix $\mathbf{V_m^{(ref)}}$ consisted of two sub-matrices each of which was calculated as described previously for the ^{234}U case.

For the neutron flux on the reference samples the covariance matrix $\mathbf{V_\Phi^{(ref)}}$ was calculated as the matrix product $\mathbf{G_\Phi} * \mathbf{V^{(ref)}} * \mathbf{G^T_\Phi}$ where $\mathbf{V}$ was the covariance matrix that constisted of the $\mathbf{V_k^{(ref)}}$ sub-matrices and $\mathbf{G_\Phi}$ was the sensitivity matrix calculated from eq. (1) and its matrix elements were $(G_\Phi)_{ij} = \partial\Phi_i^{(ref)}/\partial x_j^{(ref)}$. In this case the correlation between the fluxes in each energy was in the order of 1% and it is attributed on the sample mass. The total estimated uncertainties can be seen in Table 2.

Finally, the total estimated uncertainty of the ^{234}U(n,f) was derived from the covariance matrix $\mathbf{V_\sigma}$ which was calculated as the product $\mathbf{G_\sigma} * \mathbf{V} * \mathbf{G^T_\sigma}$ where $\mathbf{V}$ was the covariance matrix that constisted of the $\mathbf{V_k}$ sub-matrices placed as they appear in eq. (4) from left to right and from the numerator to the denominator and $\mathbf{G_\sigma}$ is the sensitivity matrix calculated from eq. (4) and its matrix elements were $(G_\sigma)_{ij} = \partial\sigma_i/\partial x_j$. The correlation estimated was less than 0.05% and the total estimated uncertainty can be seen in Table 2. The calculated covariance and correlation matrices can be seen in Table 1.

Energy (MeV)	**0.452**	**0.550**	**0.651**	**7.5**	**8.7**	**10.0**	**0.452**	**0.550**	**0.651**	**7.5**	**8.7**	**10.0**
0.452	0.0013						1					
0.550	$8\ 10^{-7}$	0.0010					$7\ 10^{-4}$	1				
0.651	$7\ 10^{-7}$	$5\ 10^{-10}$	0.0013				$5\ 10^{-4}$	$5\ 10^{-7}$	1			
7.5	0	0	0	0.054			0	0	0	1		
8.7	0	0	0	$2\ 10^{-19}$	0.052		0	0	0	$4\ 10^{-18}$	1	
10.0	0	0	0	$3\ 10^{-19}$	$3\ 10^{-19}$	0.036	0	0	0	$7\ 10^{-18}$	$7\ 10^{-18}$	1

Table 1. Covariance (left) and correlation (right) matrix of the ^{234}U(n,f) cross section. The zero elements indicate values which are smaller than 10^{-24} limited by the floating point precision.

Target	Energy [MeV]	σ [b]	Y [10^3]	f_{amp}	f_{DT}	$f_{out/in}$	f_{par}	f_{abs}	m [10^{18} atoms]	f_{MCNP}	Φ [10^7 n/cm^2]
^{235}U	0.452(8)	1.852(8)	6.2	0.03	2 10^{-4}	-	0.81(12)	10^{-5}	12.7(2)	-	3.9(3)
	0.550(8)	1.123(7)	3.7				0.60(8)				2.76(27)
	0.651(8)	1.120(6)	3.3				0.77(9)				2.34(26)
^{238}U	7.5(1)	0.993(8)	2.0		10^{-4}	0.081(8)	0.036(7)		25.0(3)	-	2.35(18)
	8.7(1)	1.016(8)	5.7			0.120(7)	0.059(9)				3.19(28)
	10.0(1)	1.010(8)	8.1			0.111(5)	0.18(1)				6.71(18)
^{234}U	0.452(8)	0.42(4)	1.1	0.07	0.12	-	0.152(10)		7.53(7)	1.30	5.1(5)
	0.550(8)	0.87(3)	1.6				0.133(14)			1.31	3.61(28)
	0.651(8)	0.99(4)	1.7				0.213(11)			1.36	3.19(10)
	7.5(1)	1.90(23)	4.2			0.073(4)	0.029(6)			2.06	4.84(50)
	8.7(1)	2.17(22)	9.7			0.117(1)	0.063(7)			2.06	6.52(52)
	10.0(1)	2.13(19)	16.3			0.113(3)	0.242(19)			2.02	13.6(21)

Table 2. Values of parameters used in the cross section calculation along with the total estimated uncertainties.The uncertainty in the raw counts (Y) is the square root of the raw counts (√Y). In the cases where none uncertainty is provided, a value of 10^{-10} was used in the covariance propagation.

RESULTS AND CONCLUSION

The ^{234}U(n,f) cross-section values as well as the corresponding uncertainties that were calculated can be seen on the third column of Table 2. The comparison between the present data and current evaluations (ENDF/B-VII.I [31], JEFF-3.2 [32], JENDL-4.0u2 [33], CENDL-3.1 [34] and ROSFOND-2010 [35]) and experimental data-sets found in EXFOR database[36] can be seen in Fig. 5 where, from ~ 10 up to ~ 30% can be seen. A more detailed comparison is reported on [22].

Additional calculations were also performed to estimate the total uncertainty in the reported cross-section and clarify the discrepancies found in literature, especially in the keV domain. At the 451 keV neutron energy a 10% uncertainty was calculated and is attributed to

the uncertainty of the parasitic factor f_{par} on the reference samples. At lower energies, neutrons are subject to more severe scattering in contrast to higher energies. This along with the high ^{235}U(n,f) cross-section and the accuracy of the Monte-Carlo simulations, justifies the higher uncertainty at this energy compared to the 6% and 4% at 550 and 651 keV, respectively which resulted in the confirmation of the data by Karadimos et al. [13]. The uncertainties reported at the MeV energies, where the parasitic contributions of low energy neutrons are expected to be much higher that the keV region, vary from 9 to 12% and are attributed to the accuracy limitation of the developed methodology described in [22].

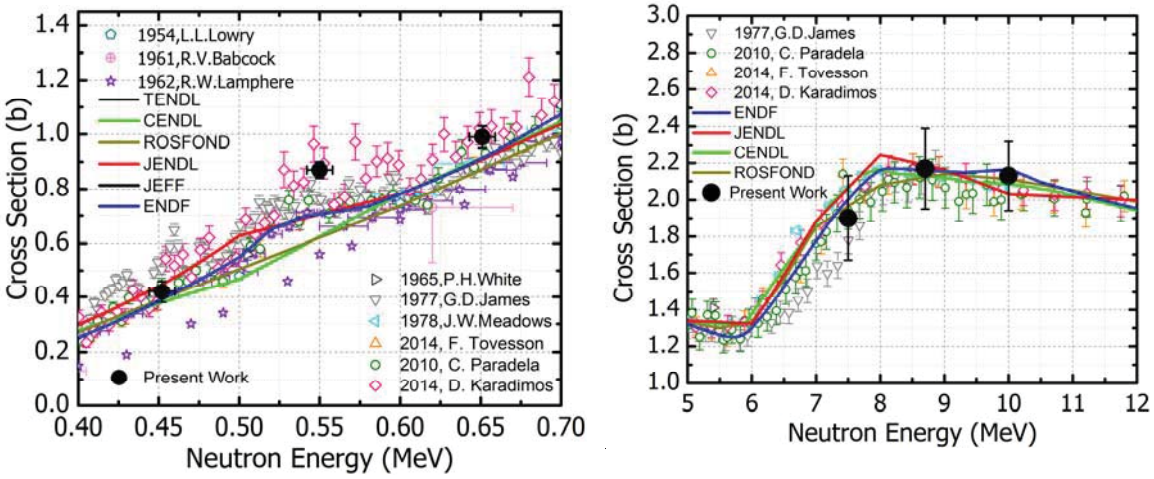

Fig. 5. Final results of the ^{234}U(n,f) cross section as calculated in this work in the kev (left) and MeV (right) energy domain with the corresponding total estimated uncertainties in comparison to available experimental data-sets and current major evaluations. It has to be noted that the reported uncertainties in the experimental data found in literature are only the statistical ones.

Acknowledgements

This research is implemented through IKY scholarships programme and co-financed by the European Union (European Social Fund - ESF) and Greek national funds through the action entitled Reinforcement of Postdoctoral Researchers, in the framework of the Operational Programme Human Resources Development Program, Education and Lifelong Learning of the National Strategic Reference Framework (NSRF) 2014–2020. The authors would like to express their deep gratitude to Dr. P. Schillebeeckx for his invaluable help in understanding the concepts of data evaluation and covariance propagation. The authors would also like to express their gratitude to Dr. V.G. Pronyaev for his help in sharing the latest evaluated neutron standards.

References

[1] IAEA, IAEA-TECDOC-1450 (2005)
[2] R. Lamphere, Phys. Rev. 91(3), 655 (1953)
[3] R. Lamphere, R. Greene, Phys. Rev. 100(3), 763 (1955)
[4] R. Lamphere, Phys. Rev. 104(6), 1654 (1956)

[5] R. Lamphere, Nucl. Phys. 38(C), 561 (1962)
[6] L. Lowry, Rept. Los Alamos Scientific Lab. No. 1714 (1954)
[7] R. Babcock, Tech. rep., Bettis Atomic Power Lab., Westinghouse, (1961)
[8] P. White et al., in Phys. and Chem. Fission Conf. Salzburg, vol. I (1965), vol. I, p. 219
[9] G.D. James, et al., Phys. Rev. C 15, 2083 (1977)
[10] J.W. Meadows, Nucl. Sci. Eng. 65(1), 171 (1978)
[11] C. Paradela, et. al., Phys. Rev. C 82, 034601 (2010)
[12] F. Tovesson, A. Laptev, T. Hill, Nucl. Sci. Eng. 178(1), 57 (2014)
[13] D. Karadimos, et. al., Phys. Rev. C 89, 044606 (2014)
[14] R. Vlastou, et. al., Nucl. Instrum. Meth. B 269(24), 3266 (2011)
[15] R. Vlastou, et. al., Physics Procedia 66, 425 (2015)
[16] S. Andriamonje, et. al, Journal of Instrumentation 5(2) (2010)
[17] S. Andriamonje, et. al., Journal of the Korean Physical Society 59(23), 1601 (2011)
[18] S. Andriamonje, et. al., IEEE Transactions on Nuclear Science 56(3), 1076 (2009)
[19] Y. Giomataris et al., NIM A 376 (1), p. 29 – 35 (1996)
[20] Y. Giomataris, NIM A 419, p. 230 – 250 (1998)
[21] Y. Giomataris, ICFA Instrum. Bul.19
[22] A. Stamatopoulos et al., EPJA (2018) 54:7
[23] A. Tsinganis et al., EPJ Web Conf. 146 (2017) 04035
[24] K.H. Schmidt et al., Nucl. Data Sheets 131, 107 (2016).
[25] A. Ferrari et al. cds.cern.ch/record/898301.
[26] D. A. Brown et al., Nucl. Data Sheets, 148 (2018) pp. 1-142
[27] J.F. Ziegler, Nucl. Instrum. Methods B 219, 1027 (2004).
[28] E. Birgersson, G. Loevestam, NeuSDesc EUR 23794 EN (Eur. Commission,2009).
[29] L. Waters et al., AIP Conf. Proc. 896, 81 (2007).
[30] A. D. Carlson et al., NDS 148 (2018) pp. 143-188
[31] M. Chadwick et al., Nucl. Data Sheets 112, 2887 (2011).
[32] JEFF-3.2: Evaluated Data Library (2014) www.oecd-nea.org/dbforms/data/eva/evatapes/jeff 32/.
[33] K. Shibata et al., Nucl. Sci. Tech. 48, 1 (2011).
[34] Z. Ge et al., J. Korean Phys. Soc. 59, 1052 (2011).
[35] ROSFOND-2010 Evaluated Data Library (2010), www.ippe.ru/podr/abbn/english/libr/rosfond. php.